FREQUENCY ACTUATION OF DIFFERENT CONCENTRATIONS IRONSPERM IN *IN VITRO* SITUATION

Lianne Weber

Faculty of Engineering Technology - Department of Biomedical Engineering

Examination committee

Dr. I. S. M. Khalil
Dr. J. Dasdemir
Dr.ir. K. Goulas

December 2023

UNIVERSITY OF TWENTE.

Abstract

Biohybrid microrobots are an emerging research area for *in vivo* applications, such as minimally invasive surgeries and local drug delivery. However, predicting the behaviour of these microrobots is challenging, multiple parameters influence the behaviour of microrobots. This paper focuses on the frequency actuation of IRONSperm with different concentrations of nanoparticles. IRONSperm is a type of nanoparticle-coated bull sperm cells and is actuated by a rotating magnetic field. The rotation magnetic field allows the biohybrid microrobot to interact with a surface resulting in a translational velocity. It is demonstrated how an increase in nanoparticles influences the cut-off frequency by looking at the translational velocity. The response showed no effect of the increase in nanoparticles on the cut-off frequency.

Contents

1 Introduction

Worldwide 18.094.716 cancer diagnoses were detected in 2020. Of which 15.3% of all female cancer cases are within the uteri or ovarian tract [1]. The current cancer treatment utilizes combinations of surgery, chemotherapy and radiation. These treatments are effective but are invasive to the patient. To make the treatments as minimally invasive as possible, current research focuses on localized chemotherapy [2]. Localized drug delivery is directly administered at the disease site. This has multiple advantages for example; a decrease in drug circulation through the body and reduced side effects; reduced medicine usage because of direct drug delivery at the site of disease; and controlled drug release to ensure drug uptake in the cancer cells [2]. However, local delivery of the drug is still a challenge.

Microrobots can be used for local drug delivery. These robots have dimensions in the mm scale and can reach parts of the human body that are difficult to reach with normal medical devices [3]. Besides drug delivery, microrobots can be used for stem cell delivery [4] and thrombus treatment [5]. Microrobots are too small to have power sources, sensors and computer circuits for movement [6]. Therefore, microrobots have been designed with various propulsion methods, such as electric field, magnetic field, light field and sound field [7]. Of these, magnetic actuation is preferred, because it is safe to use for biological tissues and has controllable, remote and long-range actuation [8, 9]. With untethered microrobots, hard-to-reach locations can be accessed due to their size and no obligation to cut the body.

When making magnetic microrobots, they should be biocompatible and cytotoxicity should be avoided. Using non-biocompatible materials, toxic substances can accumulate in the body and cause inflammatory responses [10]. A solution is using biological cells, which are more biocompatible. For example, sperm cells are natural swimmers and propel themselves using a flagellum movement. Unfortunately, the speed of the microrobot sperm cell is slower than the free-swimming sperm cells [11].

Adding artificial components can support the biological cells in their movement. Soft biohybrid microrobots are combined biological cells and artificial components, with the advantages of wireless actuation, biocompatibility, flexibility, cargo loading and adaptability [12]. Different soft biohybrid microrobots are an emerging research area and shows promising results [4, 5, 13]. Santomauro et al. added Tb^{3+} to the *Chlamydomonas reinhardtii* cells and directional actuated the *C. reinhardtii* cells by an external magnetic field [14].

Another example of biohybrid microrobots are dead bull sperm cells combined with iron oxide (Fe_3O_4) nanoparticles, called IRONSperm. It is a soft biohybrid microrobot and can magnetically be actuated [9]. Previous research showed the assembly of nanoparticles on single sperm cells [15]. This microrobot was successfully actuated and had a swimming speed of 0.2 body length/s. Besides, Magdanz et al. [15] showed that IRONSperm can successfully be loaded with medicines. This shows promising results for IRONSperm drug-delivery microrobots (Figure 1.) However, a more stable actuation and higher drug-loaded concentration is preferred.

For higher drug-loaded concentration and more stable actuation, a bigger cluster of IRONSperm was formed. A cluster of IRONSperm needs a smaller magnetic field for actuation. With cluster formation, the soft biohybrid microbot was able to roll on a surface and move forward with a smaller magnetic moment [9]. Middelhoek et al. showed proof of principle of the rolling motion of the cluster [9]. However, predicting the behaviour of these biohybrid microrobots is limited. For further development of an actuation model, different parameters can be investigated. To start, it is important to determine the cut-off frequency based on the cluster appearance. Two main conditions of the cluster appearance are size and nanoparticle concentration. In this report the goal is to find a correlation between the cluster concentration and the cut-off frequency.

Three concentrations of IRONSperm (1, 2, 3 mg/mL) will be investigated over a frequency range from 0.1 to 10 Hz. The translational velocity and cluster configuration will be received using visual feedback. Using this data, the actuation model of IRONSperm can be further devel-

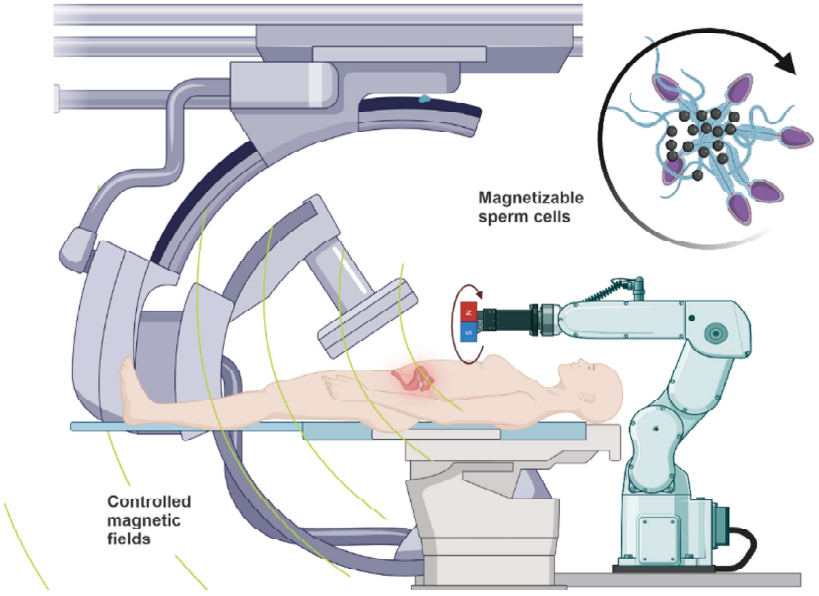

Figure 1: Biohybrid microrobots are used for minimally invasive treatment in the female reproduction tract. The microrobots made from sperm cells and nanoparticles can be controlled by a rotating magnetic field and localized with CT imaging [16].

oped. For future applications, such a model can predict the behavior of the cluster. Eventually, a controller could be made were visual input and location of the external magnet are utilized to guide the cluster along a predetermined trajectory.

2 Actuation of soft biohybrid microrobots

Magdanz et al. [15] showed electrostatically self-assembly of magnetic nanoparticles around sperm cells. Due to the positively charged nanoparticles and the negative surface charge of the sperm cell. Magnetization of the sperm cell gives an actuation field and by applying a rotating magnetic field, the biohybrid microrobot, called IRONSperm, controllably swims forward.

Single IRONSperms can entangle together due to physical interactions [9]. A rotation magnetic field gives the iron cells more physical interactions and clusters are realized. The nanoparticles are heterogeneously divided among the sperm cells and sperm cell membranes. The heterogeneous distribution provides electrostatic and magnetic interactions between single IRONSperm forming a cluster. Applied magnetic field strength, the concentration of sperm cells and nanoparticles and self-assembly time influences the cluster configuration [9]. These clusters can be approximated as soft-magnetic ellipsoids, with major axis a and minor axis b (Figure 2).

Applying an external magnetic rotation field provides wireless magnetic actuation of these biohybrid microrobots. The external magnetic field gives the IRONSperm cluster a need to align since the magnetic moment of the IRONSperm cluster results in torque if the external magnetic field is not aligned (Figure 2). The magnetic field direction θ_f and the cluster orientation θ_c influence the amount of torque received. As well as, the demagnetization factor n_a in the preferred magnetization direction of the cluster e_1 and the demagnetization factor n_r in the preferred magnetization direction of the cluster e_2.

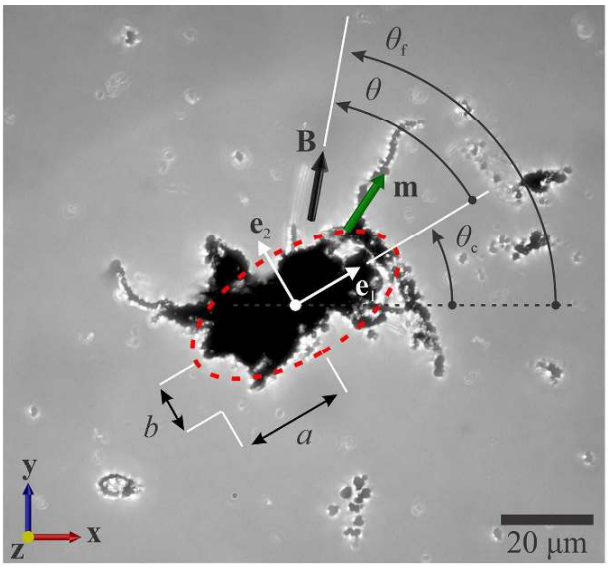

Figure 2: An IRONSperm cluster is approximated as an ellipsoid. An magnetic field and moment are acting on the cluster [9].

The cluster formation increases the magnetic moment of the microrobot compared to a single IRONSperm, resulting in a bigger magnetic torque. Magnetic torque, viscous drag torque and contact drag torque influence the rolling locomotion of the IRONSperm [9]. Magnetic torque $\boldsymbol{\tau_m}$ is given by

$$\boldsymbol{\tau_m} = \boldsymbol{m} \times \boldsymbol{B}, \tag{1}$$

with magnetic moment $\boldsymbol{m}$ and magnetic field $\boldsymbol{B}$. Also, the viscous drag torque τ_d, defined as

$$\boldsymbol{\tau_d} = f_r \boldsymbol{\omega_c}, \tag{2}$$

acts on the IRONSperm cluster, depending on the rotational drag coefficient f_r and angular velocity of the cluster ω_c. Last, there is surface drag torque $\boldsymbol{\tau_s}$, a torque exerted on the cluster

created by the drag forces of contact with the surface. Together the torque balance is given by:

$$\boldsymbol{\tau_m} + \boldsymbol{\tau_d} + \boldsymbol{\tau_s} = 0. \tag{3}$$

The cut-off frequency of the cluster is the maximum angular velocity at which the cluster does not rotate at the same rate as the external magnetic field. The cluster is approximated as a soft-magnetic ellipsoid and has a cut-off frequency ω_{co} of

$$\omega_{co} = \frac{|\boldsymbol{B}|^2 \, |n_a - n_r| \, V}{2\mu_0 n_a n_r f_r}, \tag{4}$$

with volume of the cluster V and vacuum magnetic permeability μ_0 [9]. The cut-off frequency is the frequency where the cluster is not synchronized with the magnetic field. When actuated below the cut-off frequency, the angular velocity of the cluster equals the angular velocity of the magnetic field. After the cut-off frequency, the angular velocity of the cluster is slower. When clusters are actuated above their cut-off frequency, the angular velocity decreases over time. The angular velocity of the soft-magnetic cluster is given by:

$$\omega_c = \frac{d\theta_c}{dt} = \omega_{co} sin(2(\omega_f t - \theta_c)) \tag{5}$$

with angular velocity of the magnetic field ω_f and time t. The rotation of a cluster can be used for locomotion. When the cluster is in contact with the surface, the magnetic torque causes the cluster to rotate. Since it is in contact with the surface, the surface drag will ensure the forward rolling motion of the cluster around its axis over the surface. The translational velocity v is

$$v = p\omega_f/(2\pi), \tag{6}$$

with perimeter p. In optimum circumstances, the cluster will roll without slipping and travelling the length of its perimeter in one rotation. Therefore, clusters characterized by a greater perimeter have a higher translational velocity compared to clusters with a smaller perimeter.

3 Methods

3.1 Frequency response of the clusters

IRONSperm samples is formed with electrostatic-based self-assembly proceeded by colleagues (Appendix A). Resulting in IRONSperm samples with nanoparticle concentrations of 1 mg/mL, 2 mg/mL and 3 mg/mL. The frequency response is measured for the three concentrations, each featuring two different clusters (measurement A and B). Multiple clusters for each concentration are produced. With an external magnet, it is checked if the clusters reacted on the magnet. From each concentration, the two clusters, which reacted when the magnet was furthest away are used. The clusters are sorted on size, the biggest clusters are used in measurement A and the smallest in measurement B.

A sample is placed inside a transparent perspex tube with an inner diameter of 10 mm and an outer diameter of 15 mm, filled with 0.9% saline. The RPM (rotating permanent magnet) is connected to a KUKA robotic arm and is located 50 mm above the tube (Figure 3). The RPM is a cylindrical magnet (NdFeB Grade-N45) with a height of 20.0 mm and a radius of 17.5 mm. The clusters receive a maximum magnetic field strength of 28 mT. For each trial, the permanent magnet stayed fixed. Before starting the measurements, the cluster has at least been moved back and forth once with the RPM, to ensure magnetic coupling and stable cluster shape. When coupled, the cluster is moved by the RPM with a counterclock wise rotation to the left side. The rotational direction is changed when the IRONSperm cluster has no translational velocity. The cluster moving direction is changed 6 times for each concentration. The actuation frequency of the RPM is ranging from 0.1 Hz to 10 Hz. With a step size of 0.1 Hz between 0.1 and 2 Hz and a step size of 0.5 Hz between 2 and 10 Hz. Using a FLIR Blackfly camera with Fujinon 1:1.2/6 mm lens the movement is captured in video with a framerate of 30 frames per second. The camera is placed perpendicular to the perspex tube (Figure 3). For a frequency of 1.5 Hz, a camera is placed beneath the sample and recorded the movement.

Figure 3: Wireless manipulation system of the KUKA robotic arm with a rotating magnetic field attached.

3.2 Data analysis

Using the SpinView application the cluster movement of every frequency was captured in separate videos. The line profile function in *Tracker Video Analysis and Modeling Tool* is used. The videos are loaded into the software and a frameskip of 20 is applied to reduce computing time. The intensity spectrum is determined for each frame at the y-value over which the cluster moves. Next, the pixel height is calculated within the Tracker software.

The line profiles for every 20th frame have been imported into MatLab and converted to the travelled distance. Using the filming frequency, a time-distance plot is created. The translational velocity is then calculated with the linear part of the graph. The translational velocity is further analysed with the cut-off frequency and cut-off velocity. The cut-off frequency is determined as the largest peak after which the graph stabilizes in the velocity-frequency plot. The corresponding velocity is the cut-off translational velocity of the cluster. To find a relation between the actuation and concentration, the Pearson correlation coefficient (R-value) is calculated for cut-off frequency and cut-off velocity.

Cluster shape over time is determined using the Image Processing Toolbox of MatLab. Using the side-view recordings, the cluster shape is represented using the perimeter, area and major and minor axis. The 3D approximation is calculated by a frame for the x, y and z view of the cluster each. The major and minor axes are determined for these frames. It is assumed that the clusters are ellipsoidal and a, b and c are the semi-axes. With this, the volume is calculated for en ellipsoidal. Eventually, the velocity is normalized to the perimeter and volume.

4 Results

4.1 Actuation

IRONSperm cluster is actuated with the magnetic RPM and the cluster has a rolling movement. When in contact with the top surface of the tube, the cluster rolls along the surface and moves forward (Figure 4). The cluster only rotates as the RPM rotates. The angular velocity of the cluster is translated into translational velocity if the cluster is in contact with a surface. The RPM is in the middle of the movement at a height of 5 cm. When the cluster moves towards the RPM, the cluster moves faster than the cluster past the RPM (Figure 5). During actuation, the clusters move an average of 28.5 $\pm$ 5.7 mm horizontally in the tube.

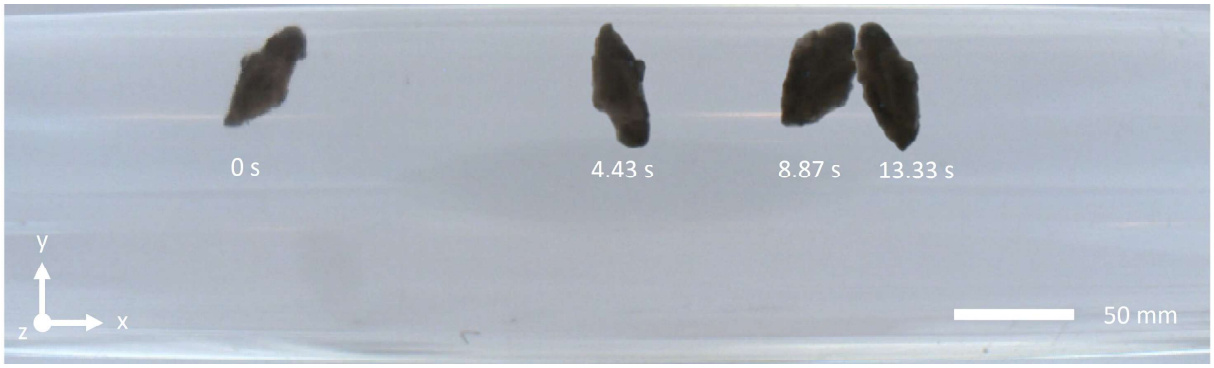

Figure 4: Actuation of an IRONSperm cluster with 2 mg/mL nanoparticle concentration at 1.5 RPM frequency. Overtime, the cluster moves along the x direction as the RPM rotates clockwise.

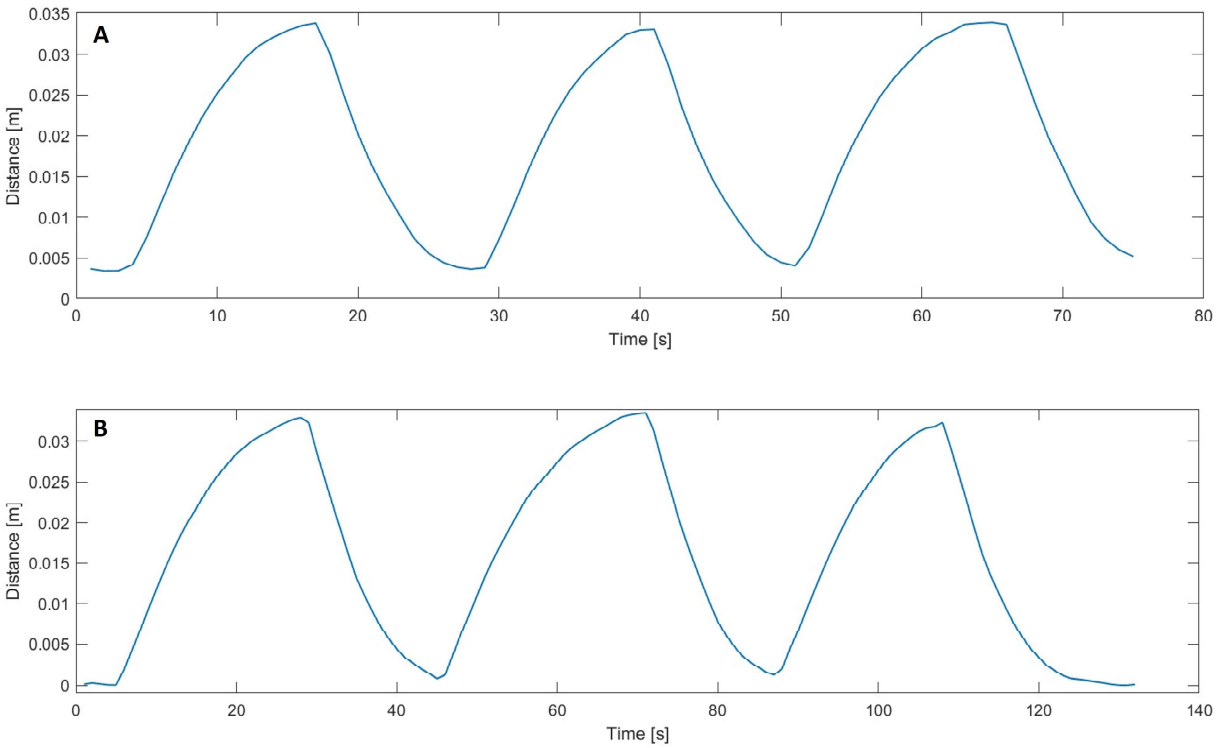

Figure 5: Travelled distance over time of the cluster with 3 mg/mL concentration. (A) Measurement A with an actuation frequency of 1.4 Hz. (B) Measurement B with an actuation frequency of 1.4 Hz.

The cluster rotates with the same frequency as the RPM till the cut-off frequency. After the cut-off frequency, the angular velocity stabilizes despite the increasing frequency of RPM. The clusters rotate along the top side of the tube. They are inconsistent in size and shape over the different measurements (Figure 6). There is a difference in size, travelled distance and time.

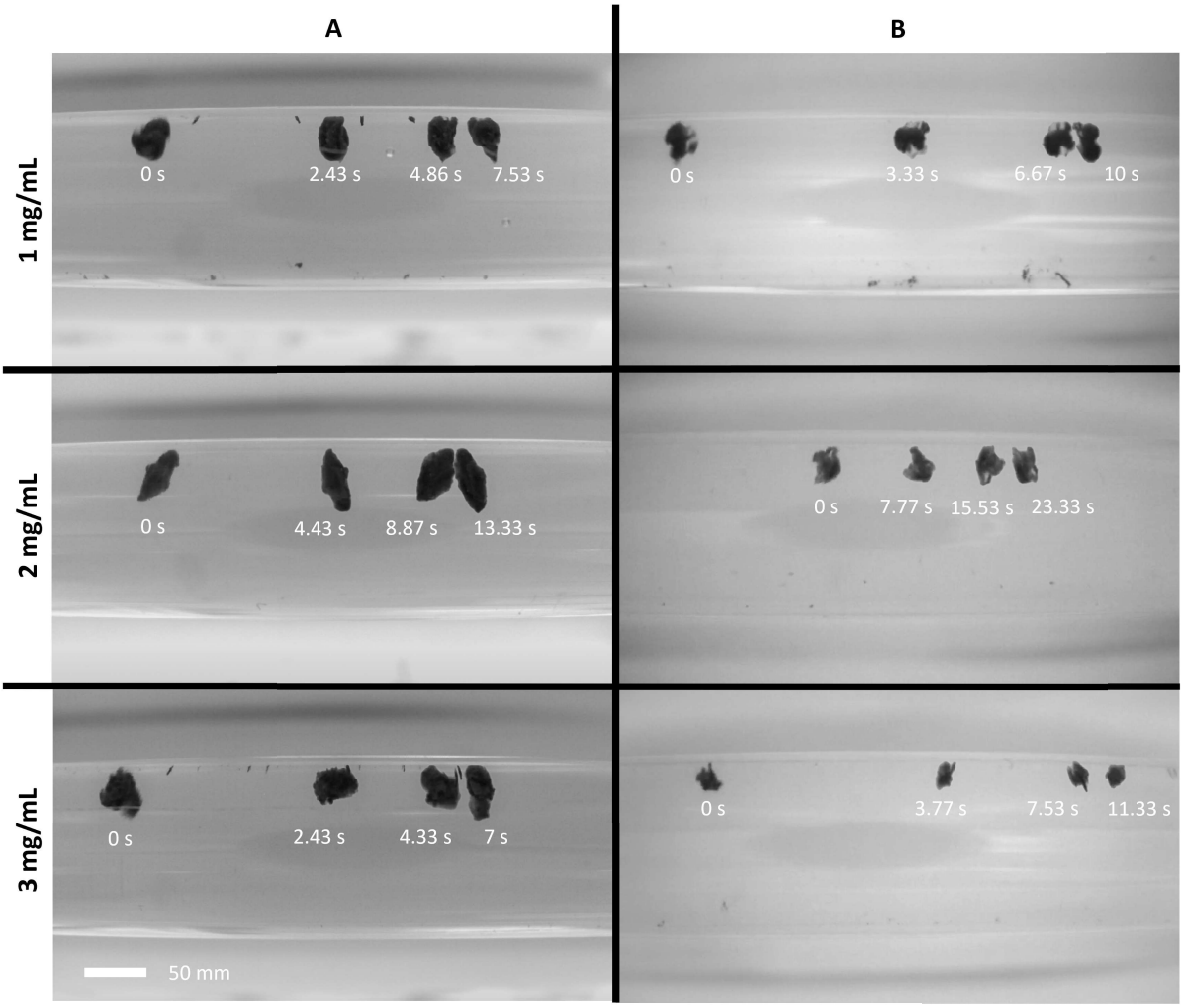

Figure 6: For measurements A and B are the IRONSperm clusters actuated at frequency = 1.5 Hz and have an angular velocity. When in contact with the wall, the angular velocity is translated into translational velocity. Moving towards the RPM, the cluster accelerates faster than moving away from the RPM. The clusters in measurement A are bigger and take less time to achieve their outer end of the movement.

4.2 Translational velocity

Up till the cut-off frequency, the translational velocity increases with actuation frequency (Figure 7). After the cut-off frequency, the clusters move with a lower angular velocity than the RPM and have a plateaued velocity. The increase in translational velocity before the cut-off frequency is faster than the expected translational velocity (Equation 6). The cluster rolls a larger distance than the perimeter and gives a higher translational velocity (Appendix B).

The average of the translational velocity after the cut-off frequency is calculated (Figure 8). The cluster with nanoparticle concentration of 1 mg/mL has, with 5.80 mm/s, the highest translational velocity after cut-off frequency. And 0.99 mm/s at concentration 2 mg/mL is the slowest moving cluster after cut-off frequency. A weak decreasing correlation with Pearson

correlation coefficient of -0.3567 is established between the concentrations and translational velocity.

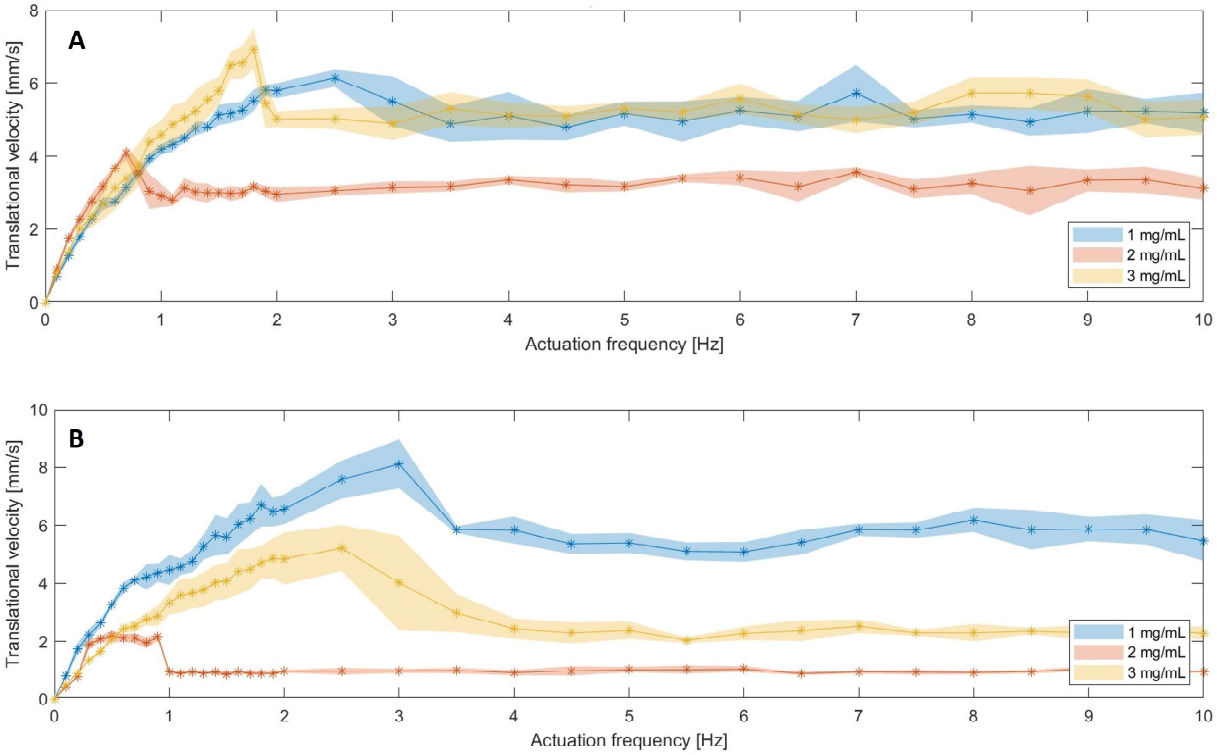

Figure 7: Increasement of the translational velocity of three different concentrations up to the cut-off frequency. After the cut-off frequency, there is stagnation. (A) In measurement A the different concentrations have the same appearance. (B) Measurement B gives bigger differences between clusters.

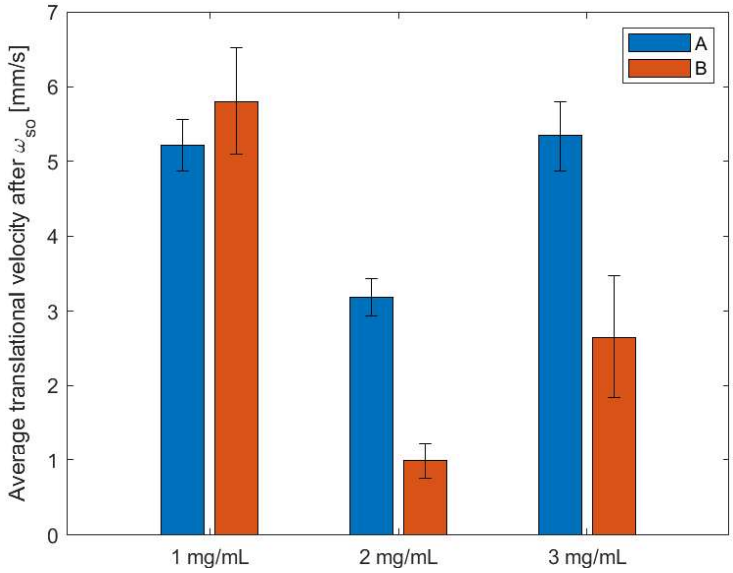

Figure 8: Average translational velocity after the cut-off frequency for different nanoparticle concentrations in measurements A and B. Between nanoparticle concentration and translational velocity is a medium decreasing correlation (R = -0.3567).

4.3 Cut-off frequency

The magnetic response of the IRONSperm cluster is described by the cut-off frequency (Table 1). The cut-off frequency has a corresponding cut-off velocity. The cut-off velocity is also the highest velocity the cluster achieves. The nanoparticle concentration of 1 mg/mL in measurement B gives the highest cut-off frequency (3 Hz) with cut-off velocity (8.11 ± 0.85 mm/s) (Figure 9). The IRONSperm cluster of 2 mg/mL in measurement A has the lowest cut-off frequency (0.7 Hz) with cut-off velocity (4.09 ± 0.19 mm/s). For the cut-off frequency as for the cut-off velocity, there is a weak decreasing correlation between concentration and cut-off.

Table 1: cut-off frequency ω_{so} and velocity v are measured for IRONSperm concentrations.

Measurement	**NP [mg/mL]**	v **[mm/s]**	ω_{so} **[Hz]**
A	1	6.13 ± 0.25	2.5
	2	4.09 ± 0.19	0.7
	3	6.93 ± 0.55	1.8
B	1	8.11 ± 0.85	3
	2	2.17 ± 0.23	0.5
	3	5.21 ± 0.80	2.5

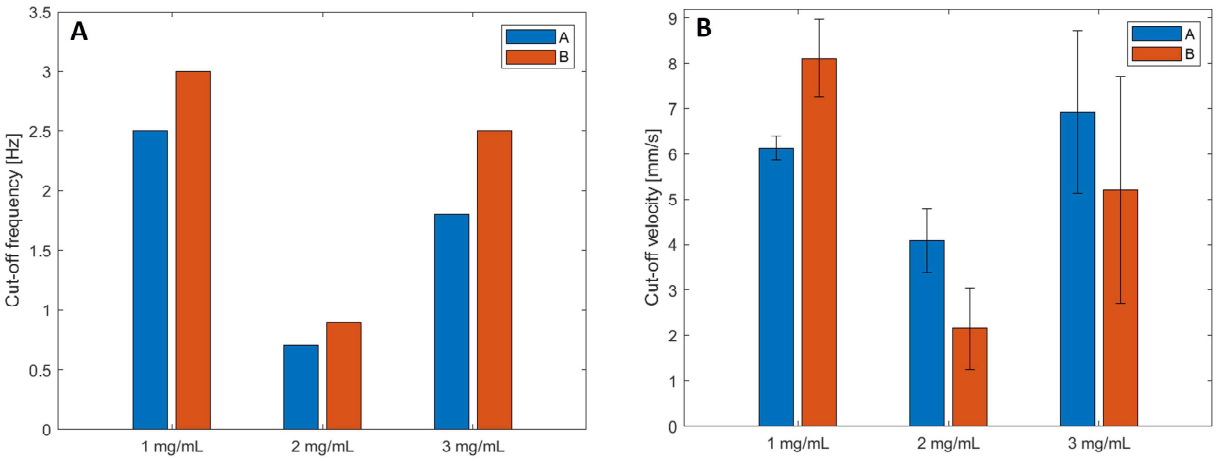

Figure 9: IRONSperm clusters have different cut-off properties for concentrations 1 mg/mL, 2 mg/mL and 3 mg/mL. (A) Cut-off frequency decreases with a weak correlation by concentration (R = -0.2867). (B) The translational velocity of the IRONSperm cluster at the cut-off frequency has a weak correlation (R = -0.2212).

4.4 Cluster shape

4.4.1 1D measurements

Change in perimeter is measured with the side view. Only sample 1 mg/mL in measurement A and 2 mg/mL in measurement B, shows change in perimeter after the cut-off frequency. The other samples don't change with increasing frequency, but the error does increase (Figure 10). The clusters in measurement A have an average perimeter of 12.65 ± 0.73 mm and the clusters in measurement B have an average perimeter of 8.12 ± 0.56 mm.

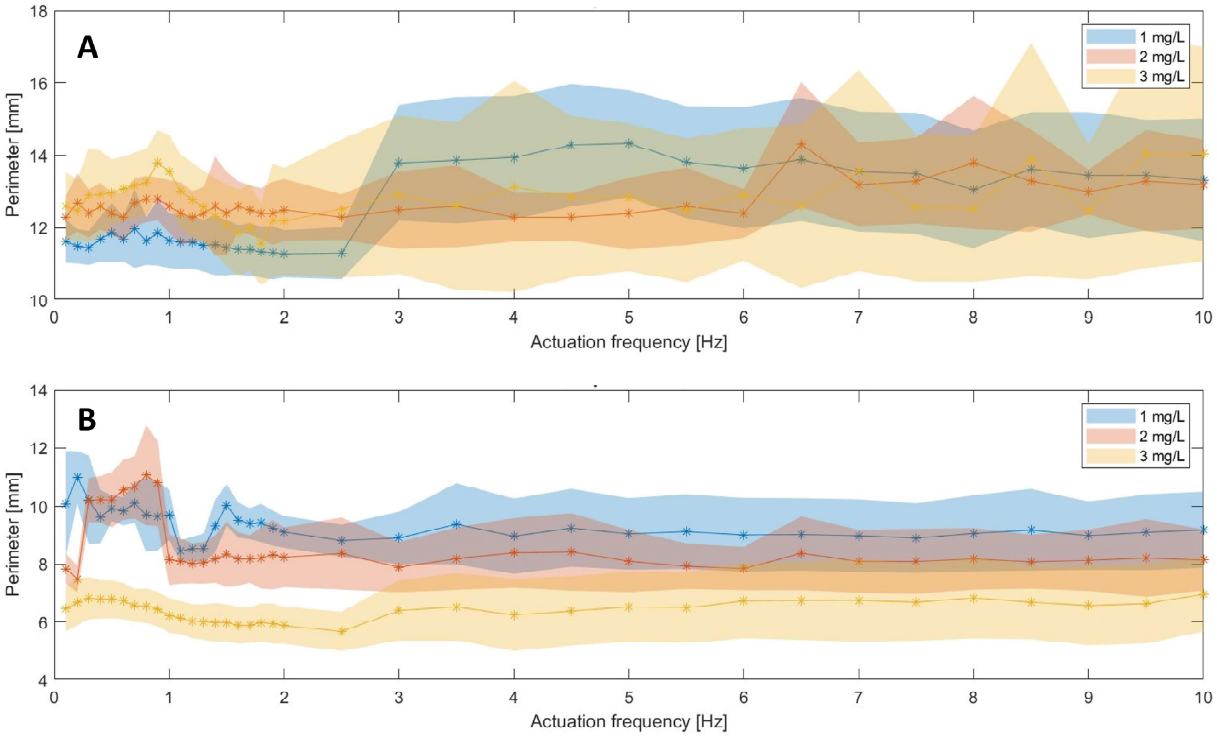

Figure 10: No correlation between IRONSperm cluster configuration in 1D side view and actuation frequency is found for any concentration. (**A**) Measurement A shows the time-averaged perimeter. The cluster with a concentration of 1 mg/mL has a change in perimeter after the cut-off frequency of 2.5 Hz. (**B**) Time-averaged perimeter in measurement B for the actuation frequency.

4.4.2 3D approximation

Besides the difference in the perimeter of the side view, there is a difference across the samples in the other axis of the approximated ellipsoid with axes a, b and c (Table 2).

Table 2: IRONSperm approximation of ellipsoid at frequency = 1.5 Hz.

Measurement	**NP [mg/mL]**	a **[mm]**	b **[mm]**	c **[mm]**	V **[10^{-2} mm^3]**
A	1	4.70	2.31	1.69	7.68
	2	4.16	1.30	2.83	6.43
	3	4.72	2.18	1.68	7.27
B	1	2.85	1.77	1.16	2.45
	2	1.842	1.33	1.10	1.12
	3	2.49	1.27	0.92	1.22

4.5 Normalization

4.5.1 Normalization by perimeter

Since the concentration does not influence the actuation response of the cluster, the assumption is that larger clusters travel faster than smaller clusters (Equation 6). The translational velocity is normalized to the perimeter around which the cluster travels (Figure 11). For measurement A the difference between the three samples decreases, but still no correlation is found (Figure 12).

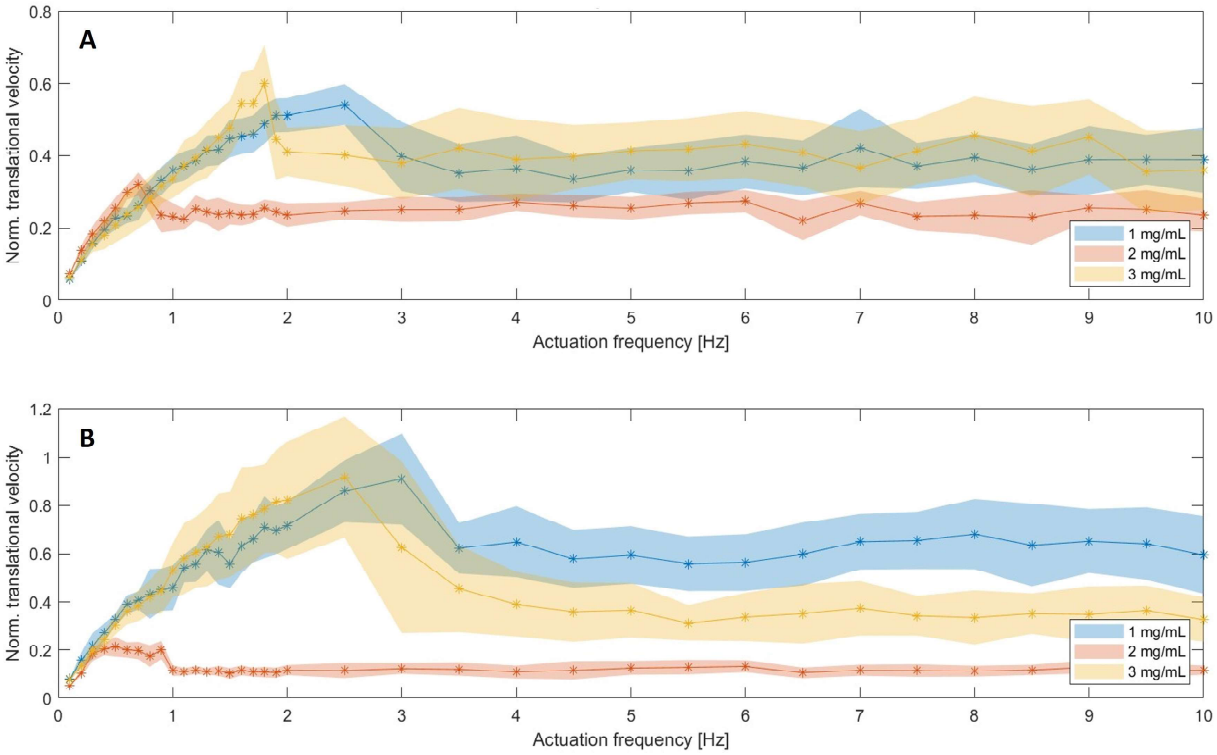

Figure 11: Normalization of the translational velocity for measurement A and B. Normalized by the perimeter for each frequency.

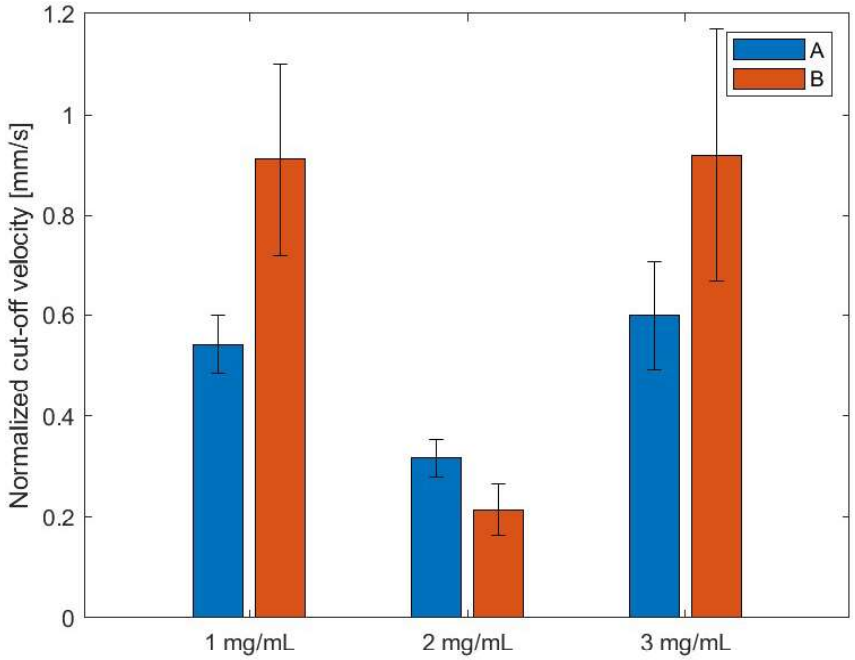

Figure 12: The cut-off velocity normalized to the perimeter for measurements A and B. There is no correlation found between the normalized cut-off velocity and the concentration (R = 0.0496).

4.5.2 Normalization by volume

Normalization with the volume shows a smaller difference between the concentrations for measurement A (Figure 13, 14). But over all the normalized cut-off velocities, there is a weak

increasing correlation found (R = 0.1664).

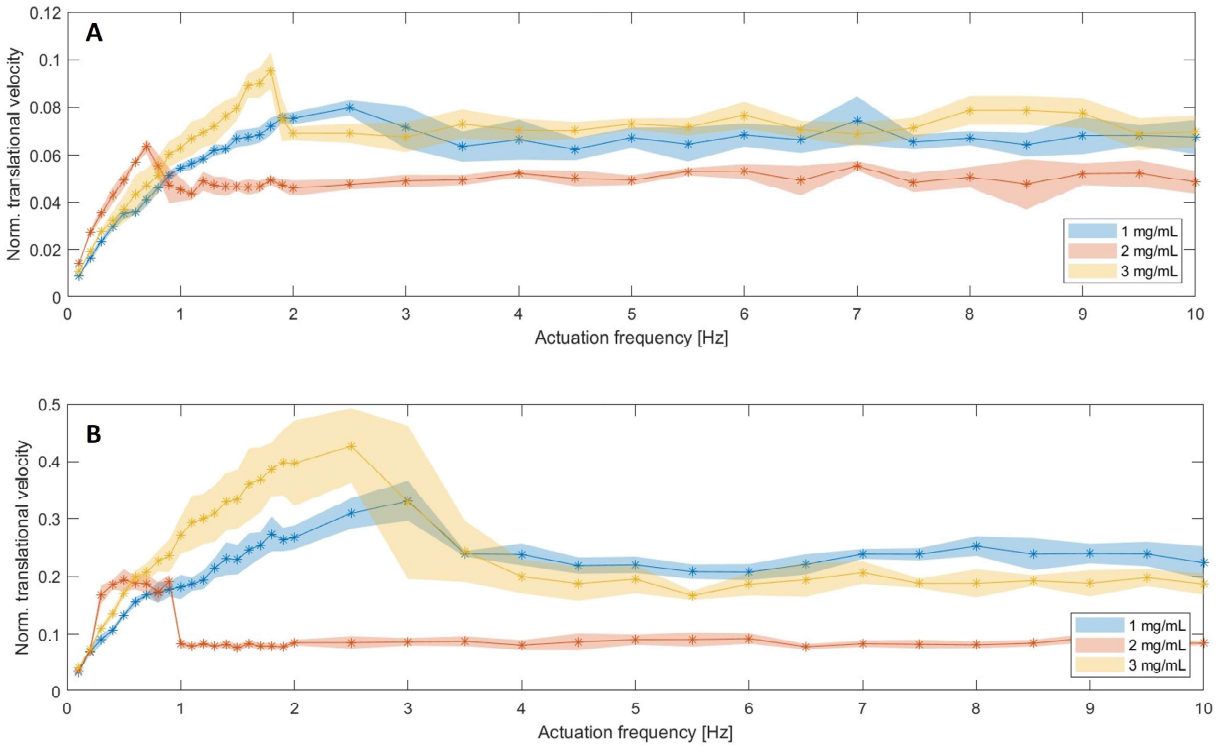

Figure 13: Normalization of the translational velocity over frequency increase for measurement A and B. Normalized by the average volume of the cluster over all frequencies.

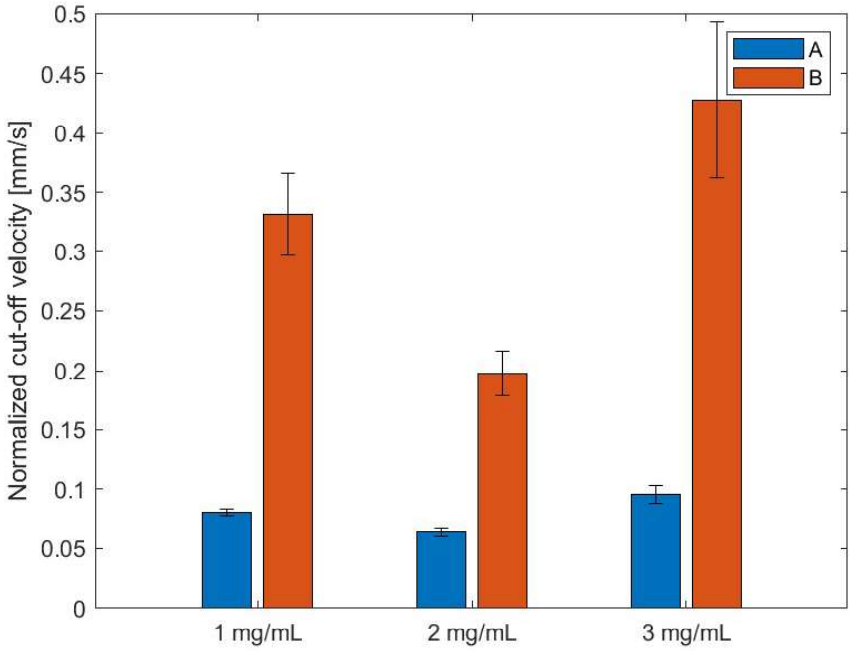

Figure 14: Normalization of the cut-off velocity for measurement A and B. Normalized by the average volume of the cluster over all frequencies. Between the normalized cut-off velocity and the concentration is a weak increasing correlation (R = 0.1664).

5 Discussion

5.1 Fabrication

The received biohybrid microrobots react differently on an external magnet when the microrobots are in the vails. Some vails showed no functionality anymore and were not clustered anymore. Therefore, two working clusters have been selected beforehand for each concentration. On top of that, all vails of each concentration contain the same amount of nanoparticles and sperm cells. However, the clusters differ in size. And thus the density of the clusters differs across samples. This influences the drag forces and the actuation.

5.2 Actuation

The clusters move due to the alignment with the magnetic field. The cluster can be seen as another small magnet, which wants to align in the magnetic field of the RPM. Since the RPM is rotating, the cluster will also rotate. Besides the rotation, the cluster is in contact with a surface. The surface drag force and the rotational force result in a translational velocity of the cluster.

The clusters only have a translational velocity when the cluster is in contact with the surface. When there is no contact, the cluster is only rotating. Therefore, the magnetic force has to be sufficient enough to pull the cluster to the top of the tube. The cluster can be moved on the bottom surface, but the cluster has to be rotated in the other direction, to travel in the same orientation of the translational velocity. This is due to the different contact locations on the cluster. To achieve rolling on the bottom, there is a small working area. The magnetic field has to be strong enough to allow the cluster to rotate. However, the magnetic attraction force has to be smaller than the gravity force, so the cluster stays on the bottom.

Looking at Figure 5, the travelled distance decreases with the position. When the cluster passes the RPM, the cluster decreases speed. The magnetic attraction force works against the movement. The cluster moves less than the perimeter during one rotation (Equation 6). This also applies the other way around, the cluster is moving towards the RPM, and the magnetic attraction force works with the translational velocity. The cluster is moving faster than the perimeter during one rotation. This influence can be reduced by a smaller magnetic field. However, the magnetic field has to be large enough to roll on the top.

As seen in Figure 6, the cluster of 2 mg/mL in measurement B moves the smallest distance. The clusters in measurement B are smaller with a factor of 2.5 compared to measurement A (Table 2). But clusters with concentrations 1 mg/mL and 3 mg/mL do not show a difference in travelled distance. The shape of the cluster differs across the clusters in all samples. However, the volume of the cluster with 2 mg/mL concentration differs only 1.4% to the volume of the cluster with 3 mg/mL concentration compared to the cluster volume in measurement A. Therefore, the difference in volume does not explain the contrast in travelled distance.

The difference in magnetization might explain the disparity. If the protocol for production is followed, no difference would theoretically be present in magnetization. However, the magnetization of the clusters is not measured and thus not guaranteed.

5.3 Translational velocity and cut-off frequency

The translational velocity graphs resulted in the cut-off frequency, the average velocity after cut-off and the cut-off velocity. The translational velocity before the cut-off frequency should be the same as Equation 6. But as seen the translational velocity is faster than the theoretical velocity. For each frequency, the translational velocity is determined for the linear part of the distance-time plot. Here the magnetic attraction force works in favour of the cluster, described in 5.2 Actuation. Therefore, the translational velocity is larger than the theoretical velocity.

The velocity at the cut-off frequency is the highest achieved translational velocity for every cluster. Here, the cluster is coupled with the RPM. Therefore, the cluster still rotates with the angular velocity of the translational velocity. This enhances the cluster movement. After the cut-off frequency, the cluster is decoupled and rotates with a smaller rotational velocity than the RPM. After the cut-off frequency, the translational velocity is stabilized. Even though the RPM's angular velocity increases, the cluster's angular velocity and translational velocity do not change. As the angular velocity does not change, the viscous drag torque also stays the same (Equation 2). Therefore, there will be an equilibrium between the magnetic and surface drag torque. Since the magnetic torque does not change with an increase in frequency, the surface drag torque does not change either (Equation 3). As all torque stabilizes, the system stabilizes and therefore the translational velocity stabilizes.

It was assumed, there is a linear correlation between concentration and cut-off frequency. With a higher concentration of nanoparticles, there is a higher coupling with the magnet. Better coupling should result in a higher cut-off frequency. But the results do not show a linear increasing correlation. On the contrary, Figure 9 shows a small decreasing correlation. An increase in nanoparticles will not always ensure the improvement of the system. One of the reasons can be a decrease in entanglement and thus decrease in density. Besides, the clusters of 2 mg/mL might not be the best representation of the concentration. The concentration of 2 mg/mL has the lowest cut-off frequency. Before the measurements were made, the attraction to an external magnet was looked at. For 1 and 3 mg/mL, the best-reacted cluster with the magnet are used. However, the used clusters of 2 mg/mL were the only ones working. This might be an error in production.

5.4 Cluster shape and normalization

The clusters showed a small decreasing correlation with the concentration. However, the concentration is not the only difference across the clusters. A big influence on the translational velocity can be the shape and volume, such as the difference in the viscous drag. Therefore, the cluster is described in multiple shape-dependent parameters.

First, the perimeter showed a change around the cut-off frequency. After the cut-off frequency, the cluster is not coupled to the magnet. Therefore, the cluster can rotate around its y-axis instead of the z-axis (Figure 4). Other sides of the cluster are then visible and change the measurement. This is also the reason why the error increases after the cut-off frequency. The perimeter does not change with the frequency.

Since the translational velocity depends on the perimeter (Equation 6), it has been normalized. This normalization showed a smaller correlation for the cut-off velocity, compared to the non-normalized cut-off velocity. But not only the perimeter but also the shape influences the translational velocity since it influences the viscous drag. During the measurements, only the side view has been captured for all frequencies. The bottom view has been captured just for 1.5 Hz. The volume is calculated with an elliptic approximation, but this does not take the different shapes of the sides into account (Appendix C). The normalization by volume of the clusters did show a small increasing correlation for the cut-off frequency.

The normalization by perimeter and volume showed no significant difference between the actuation of the concentrations. There is a medium decreasing correlation found for the cut-off frequency and a small increasing correlation for the normalization. There is an assumption, that the found cut-off frequency is correlated with the size of the cluster rather than the concentration. In Appendix D only the volume has been taken into account for the cut-off frequency and translational velocity after the cut-off frequency. The data set is insignificant for any outcome.

5.5 Reccommondations

Future experiments should help find a model for the clusters on the frequency for clinical application. It is needed to find parameters that influence the behaviour of the biohybrid microrobots. The frequency range up to the cut-off frequency is most important, since this range will be used for the locomotion through a vascular system.

Besides the concentration, the size should theoretically influence the behaviour (Equation 4). This needs to be experimentally supported. The current inconclusive representation of cut-off frequency against volume (Appendix D) has to be expanded. To receive a more robust data set and account for potential variations, the number of clusters should minimally be tripled. Next to size, there is the assumption, the shape also influences the cluster. Current clusters were not able to be changed in shape, as Magdanz et al. showed [17]. Current IRONSperm clusters use different nanoparticles ensuring more entanglement and stable cluster shape. Different cluster shapes result in different drag forces and thus other behaviour of the microrobots. Within the fabrication process and the actuation process, it can be examined how the shape of the clusters can be influenced. Preferably, looking into more sphere-like clusters. A larger cluster will then fit in a vessel, and more drugs can be targeted to a specific location. Eventually, the clinical application has to be tested. Before that happens, the response for moving against gravity; having a different magnetic field; and moving in body fluids has to be examined.

6 Conclusion

In conclusion, research on the frequency actuation of biohybrid microrobots has provided insight into their behaviour and performance. The most surprising observation is the lack of a correlation between the different concentrations of nanoparticles and the cut-off frequency. This suggests that other factors have a crucial role in determining the cut-off frequency for IRONSperm clusters. Furthermore, the clusters were cohesively and did not leave any components behind. This enhances the stability of the IRONSperm system, showing potential for a robust and reliable microrobot. Looking ahead, the biohybrid microrobots' behaviour has to be further exploited. All in all, IRONSperm clusters have the potential for further innovation and contribution to the ongoing research of microrobots.

References

[1] Cancer today; 2023. [Online; accessed 20. Oct. 2023].

[2] Wolinsky JB, Colson YL, Grinstaff MW. Local Drug Delivery Strategies for Cancer Treatment: Gels, Nanoparticles, Polymeric Films, Rods, and Wafers. Journal of controlled release: official journal of the Controlled Release Society. 2012 Apr;159(1). doi:10.1016/j.jconrel.2011.11.031.

[3] Sitti M, Ceylan H, Hu W, Giltinan J, Turan M, Yim S, et al. Biomedical Applications of Untethered Mobile Milli/Microrobots. Proc IEEE. 2015 Feb;103(2):205-24. doi:10.1109/JPROC.2014.2385105.

[4] Jeon S, Park SH, Kim E, Kim Jy, Kim SW, Choi H. A Magnetically Powered Stem Cell-Based Microrobot for Minimally Invasive Stem Cell Delivery via the Intranasal Pathway in a Mouse Brain. Adv Healthcare Mater. 2021 Oct;10(19):2100801. doi:10.1002/adhm.202100801.

[5] Lee S, Lee S, Kim S, Yoon CH, Park HJ, Kim Jy, et al. Fabrication and Characterization of a Magnetic Drilling Actuator for Navigation in a Three-dimensional Phantom Vascular Network. Sci Rep. 2018 Feb;8(3691):1-9. doi:10.1038/s41598-018-22110-5.

[6] Tumbling Microrobots for Future Medicine; 2019. [Online; accessed 10. Nov. 2023].

[7] Shen H, Cai S, Wang Z, Ge Z, Yang W. Magnetically driven microrobots: Recent progress and future development. Mater Des. 2023 Mar;227:111735. doi:10.1016/j.matdes.2023.111735.

[8] Yang Z, Zhang L. Magnetic Actuation Systems for Miniature Robots: A Review. Adv Intell Syst. 2020 Sep;2(9):2000082. doi:10.1002/aisy.202000082.

[9] Middelhoek KINA, Magdanz V, Abelmann L, Khalil ISM. Drug-Loaded IRONSperm clusters: modeling, wireless actuation, and ultrasound imaging. Biomed Mater. 2022 Sep;17(6):065001. doi:10.1088/1748-605X/ac8b4b.

[10] Wang X, Qin XH, Hu C, Terzopoulou A, Chen XZ, Huang TY, et al. 3D Printed Enzymatically Biodegradable Soft Helical Microswimmers. Adv Funct Mater. 2018 Nov;28(45):1804107. doi:10.1002/adfm.201804107.

[11] Singh AV, Ansari MHD, Mahajan M, Srivastava S, Kashyap S, Dwivedi P, et al. Sperm Cell Driven Microrobots—Emerging Opportunities and Challenges for Biologically Inspired Robotic Design. Micromachines. 2020 Apr;11(4):448. doi:10.3390/mi11040448.

[12] Schmidt CK, Medina-Sánchez M, Edmondson RJ, Schmidt OG. Engineering microrobots for targeted cancer therapies from a medical perspective. Nat Commun. 2020 Nov;11(5618):1-18. doi:10.1038/s41467-020-19322-7.

[13] Qiao S, Ouyang H, Zheng X, Qi C, Ma L. Magnetically actuated hydrogel-based capsule microrobots for intravascular targeted drug delivery. J Mater Chem B. 2023 Jul;11(26):6095-105. doi:10.1039/D3TB00852E.

[14] Santomauro G, Singh AV, Park BW, Mohammadrahimi M, Erkoc P, Goering E, et al. Incorporation of Terbium into a Microalga Leads to Magnetotactic Swimmers. Adv Biosyst. 2018 Dec;2(12):1800039. doi:10.1002/adbi.201800039.

[15] Magdanz V, Khalil ISM, Simmchen J, Furtado GP, Mohanty S, Gebauer J, et al. IRONSperm: Sperm-templated soft magnetic microrobots. Sci Adv. 2020 Jul;6(28). doi:10.1126/sciadv.aba5855.

[16] Magdanz V, Pervez Y, LaBrash-White M, Bloxs M, Mohsenkani S, Gorbet M, et al. In proceedings; Sperm Cell Empowerment: X-Ray-Guided Magnetic Fields for Enhanced Actuation and Localization of Cytocompatible Biohybrid Microrobots; 2023. .

[17] Magdanz V, Cumming J, Salamzadeh S, Tesselaar S, Alic L, Abelmann L, et al. In proceedings; Influence of Nanoparticle Coating on the Differential Magnetometry and Wireless Actuation of Biohybrid Microrobots. 2023 07.

A Biohybrid microrobot assembly

Nanoparticle-coated bull sperm cells are fabricated by electrostatic-based self-assembly [9]. The iron oxide nanoparticles (Fe_3O_4) are fabricated from a redox reaction of $FeCl_3$, $FeCl_2$ and NH_4OH. The charge of the nanoparticles and magnetization of the nanoparticles are checked (Figure 15A-B). This showed high magnetization of the iron oxide particles and a big population of negatively charged nanoparticles. The local surface charges of the bull sperm will allow assembly with the nanoparticles [16].

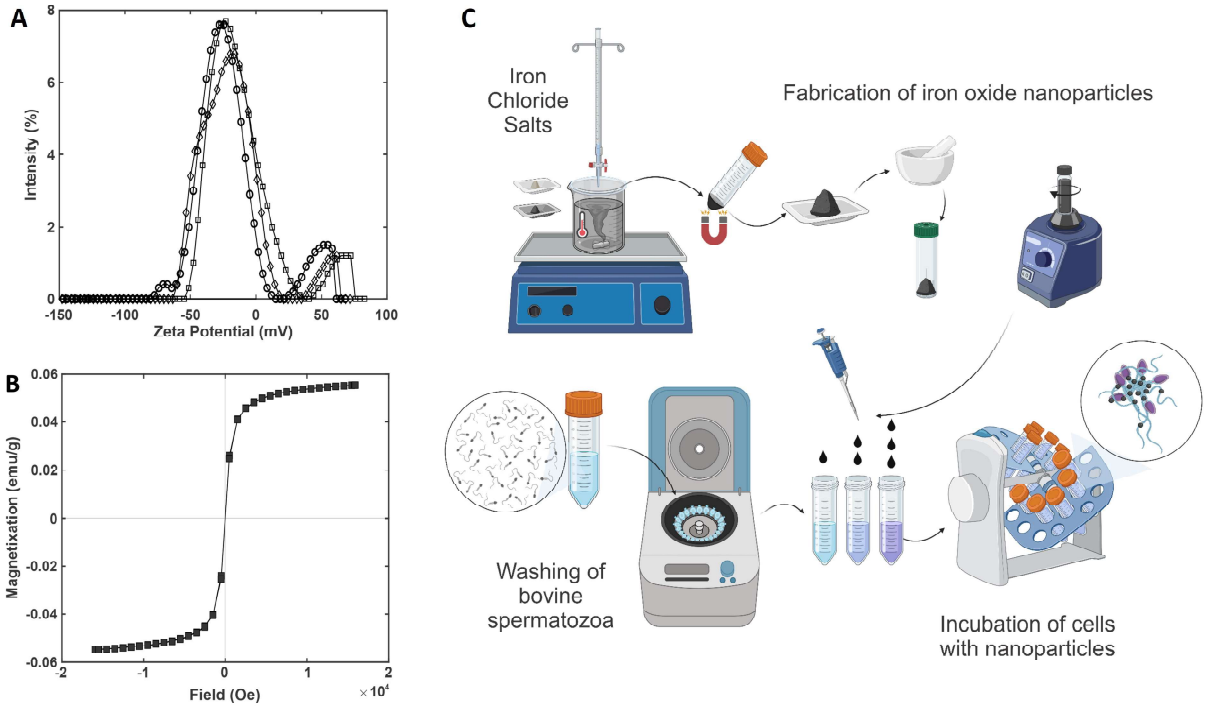

Figure 15: Biohybrid microrobot fabrication from iron chloride salts nanoparticles. The iron oxide (Fe_3O_4) nanoparticles are characterized before the fabrication of biohybrid microrobots. (A) The zeta potential of magnetic iron oxide nanoparticles shows mostly negatively charged particles. (B) The nanoparticles have a high magnetization.

Eventually, 50 μL of iron oxide (Fe_3O_4) nanoparticles solution 10 mg/mL is added to the first tube, 100 μL to the second and 150 μL to the third (Figure 15C). 350μL solution of sperm cells 2.5×10^7 cells/mL is added to all microcentrifugation tubes and filled with distilled water to a total volume of 500μL. Resulting in nanoparticle concentrations of 1 mg/mL, 2 mg/mL and 3 mg/mL combined with the sperm [16].

The sperm cells with nanoparticles entangle due to physical interactions. But to further assemble a cluster, an external rotating magnetic field is applied [9].

B Translational velocity before cut-off frequency

Equation 6 shows the velocity is dependent on the perimeter of the cluster. The measured data is bigger than the theoretical velocity (Figure 16).

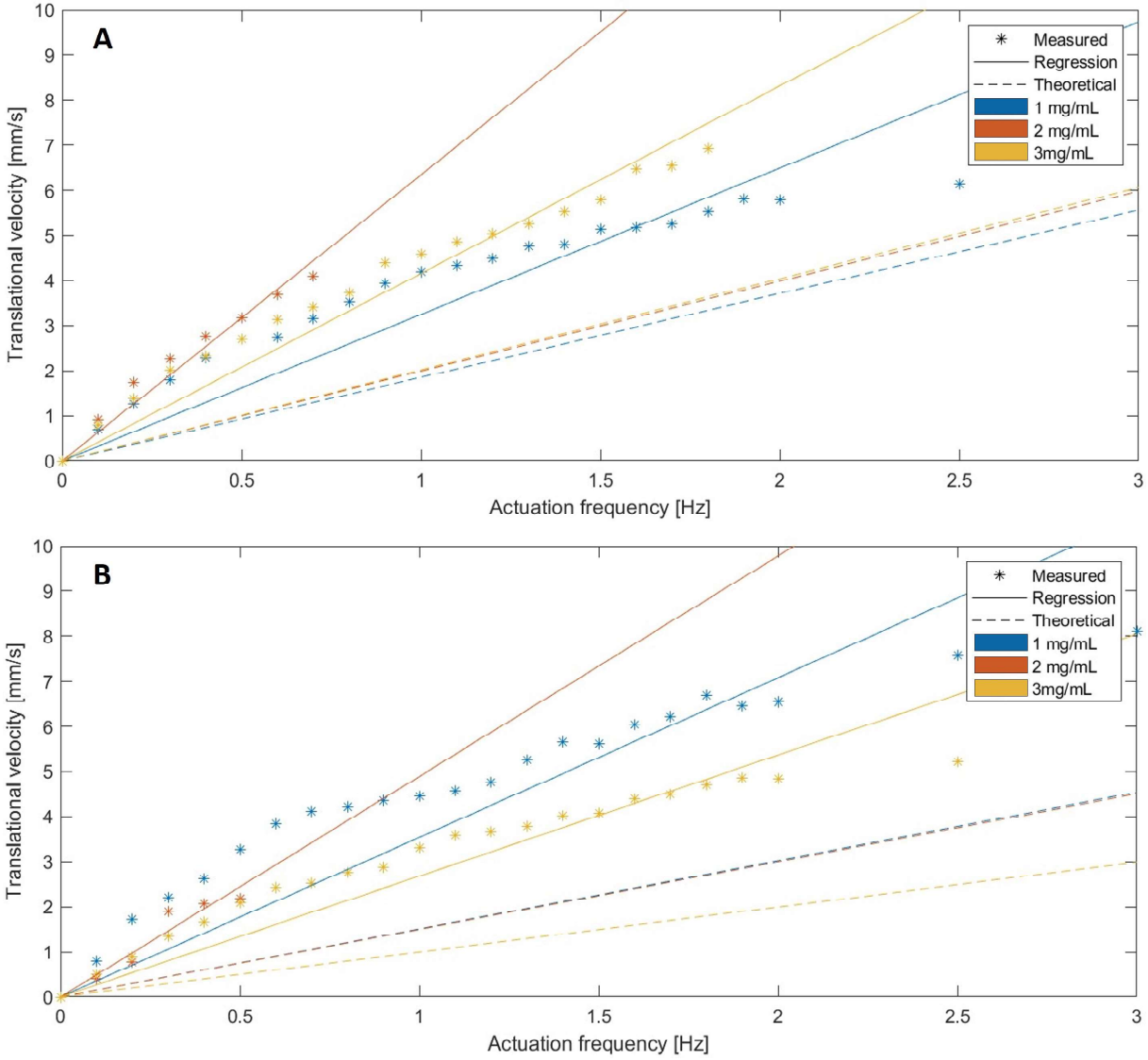

Figure 16: The measured velocity before the cut-off frequency for measurements A and B, with a regression line through the origin. The translational velocity is 1.8-3.3 times bigger than the theoretical velocity.

C Cluster shapes for 3D approximation

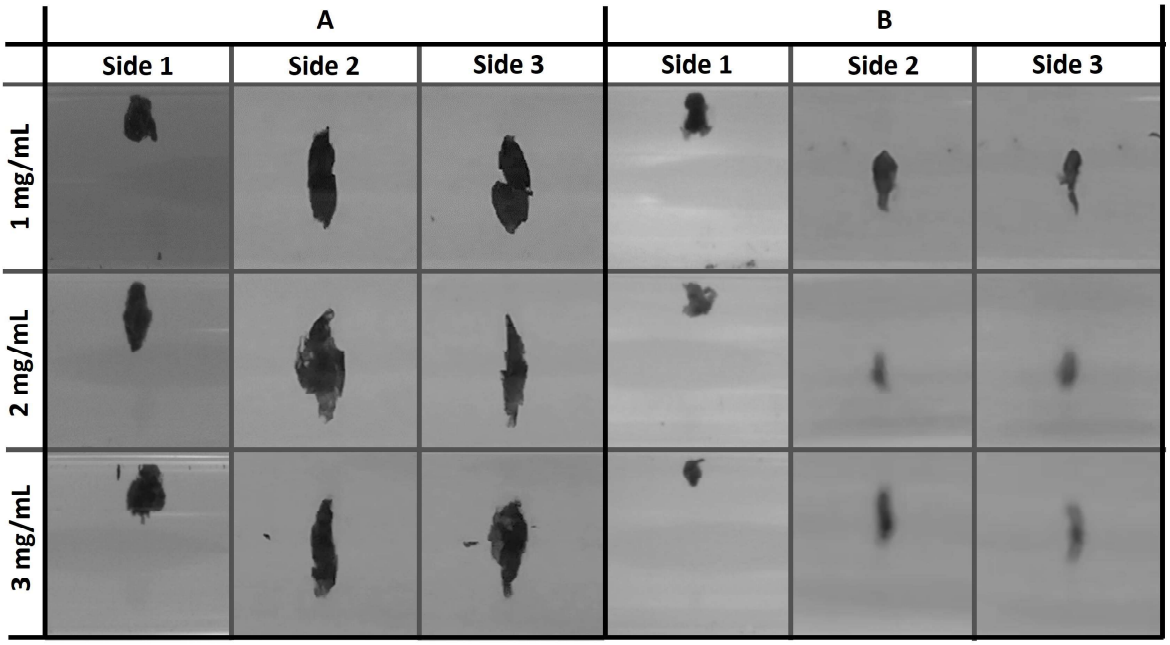

Figure 17: All 3 sides from the cluster used for the 3D approximation at frequency 1.5 Hz. Side 1 is the front view and side 2 and 3 are different bottom views. Measurement A had larger clusters than measurement B.

D Regression lines for shape-dependent cut-off frequency

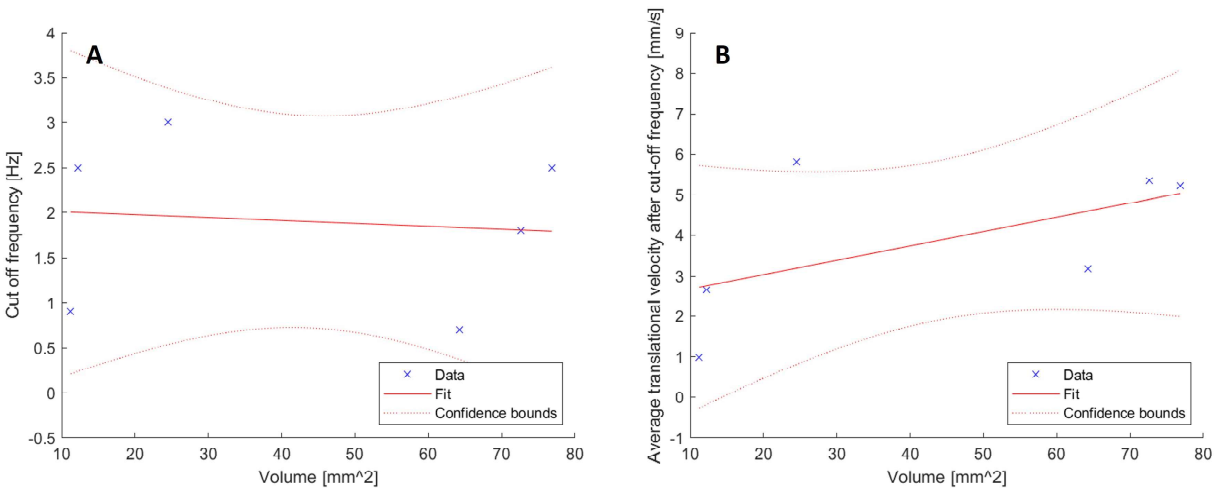

Figure 18: Assumption that the cut-off frequency and velocity is dependent on the volume. (A) Regression line of cut-off frequency and volume. (B) A regression line through the cut-off velocity after the cut-off frequency and volume shows en increase in velocity over volume.